NANO LETTERS

Letter

pubs.acs.org/NanoLett

Charging/Discharging Nanomorphology Asymmetry and Rate-Dependent Capacity Degradation in Li–Oxygen Battery

Akihiro Kushima,[†] Tetsuya Koido,[‡] Yoshiya Fujiwara,[‡] Nariaki Kuriyama,[§] Nobuhiro Kusumi,[‡] and Ju Li*[,†,∥]

[†]Department of Nuclear Science and Engineering, Massachusetts Institute of Technology, Cambridge, Massachusetts 02139, United States

[‡]Honda R&D Co. Ltd., Automobile R&D Center, Wako-shi, Saitama 351-0193, Japan

[§]Honda R&D Co. Ltd., Fundamental Technology Research Center, Wako-shi, Saitama 351-0188, Japan

[∥]Department of Materials Science and Engineering, Massachusetts Institute of Technology, Cambridge, Massachusetts 02139, United States

Supporting Information

ABSTRACT: Liquid-cell in situ transmission electron microscopy (TEM) observations of the charge/discharge reactions of nonaqueous Li–oxygen battery cathode were performed with ~5 nm spatial resolution. The discharging reaction occurred at the interface between the electrolyte and the reaction product, whereas in charging, the reactant was decomposed at the contact with the gold current collector, indicating that the lithium ion diffusivity/electronic conductivity is the limiting factor in discharging/charging, respectively, which is a root cause for the asymmetry in discharging/charging overpotential. Detachments of lithium oxide particles from the current collector into the liquid electrolyte are frequently seen when the cell was discharged at high overpotentials, with loss of active materials into liquid electrolyte ("flotsam") under minute liquid flow agitation, as the lithium peroxide dendritic trees are shown to be fragile mechanically and electrically. Our result implies that enhancing the binding force between the reaction products and the current collector to maintain robust electronic conduction is a key for improving the battery performance. This work demonstrated for the first time the in situ TEM observation of a three-phase-reaction involving gold electrode, lithium oxides, DMSO electrolyte and lithium salt, and O_2 gas. The technique described in this work is not limited to Li–oxygen battery but also can be potentially used in other applications involving gas/liquid/solid electrochemical reactions.

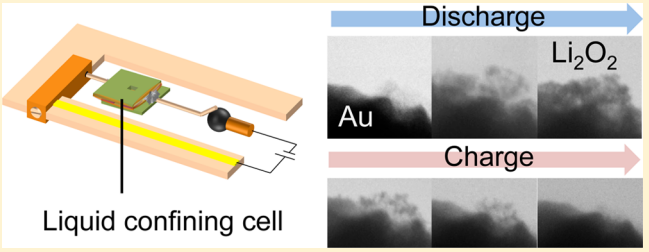

KEYWORDS: *in situ, transmission electron microscopy (TEM), liquid cell, electrochemistry, three-phase boundary*

Nonaqueous Li–oxygen battery (LOB) has an exceptionally high theoretical capacity of 3.5 kWh/kg based on the cathode-side reaction $2(Li^+ + e(U)) + O_2 \leftrightarrow Li_2O_2$ with equilibrium potential $U^0 = 2.96$ V versus lithium metal anode.[1−3] However, there are numerous technical challenges that need to be overcome.[2] These include high overpotential and low energy efficiency,[4−6] low charging/discharging rate,[7−9] and poor cycle life.[5,10,11] The asymmetry between charging and discharging processes is especially noteworthy. In ether-based electrolyte, the oxygen reduction reaction (ORR) during discharge involves superoxide O_2^- intermediate, whereas it is not observed in the oxygen evolution reaction (OER) during charging,[12] indicating different chemical pathways. There is also asymmetry in the voltage, in that the overpotential during charging ($\Delta U \sim 1$ to 1.5 V) is *much larger* than the overpotential during discharging ($\Delta U \sim -0.3$ V). In this work, we reveal yet another asymmetry, which resides in the morphological evolution of the electroactive primary discharge product Li_2O_2.[13] Our observation reveals that in discharging, the Li_2O_2 grows at the Li_2O_2/electrolyte interface (often in a dendritic fashion); but in charging, the Li_2O_2 shrinks at the root instead, at the Li_2O_2/current collector interface. This tends to weaken the adhesion and reduce the true contact area between the Li_2O_2 root and the current collector, which makes the reaction self-limiting and contributes to the large overpotential. The "big body, small feet" Li_2O_2 are also seen to be swept into the liquid electrolyte upon minute flow agitations in the liquid, which may exist in real battery operations with electrode volume changes and electrocapillary effects. The insoluble Li_2O_2 "flotsams" without electrical contact is expected to be a cause of battery degradation and poor cyclability.

In situ transmission electron microscopy (TEM) is a powerful tool for probing nanoscale electrochemical reactions in real time.[14,15] Zhong et al. conducted in situ TEM study for

Received: September 21, 2015
Revised: November 1, 2015
Published: November 4, 2015

DOI: 10.1021/acs.nanolett.5b03812
Nano Lett. 2015, 15, 8260–8265

the OER of Li_2O_2 supported on multiwall carbon nanotube (MWCNT) using an all-solid setup in vacuum and revealed the reaction preferentially took place at the Li_2O_2/MWCNT interface, indicating the electronic conductivity is the limiting factor during charging.[16] However, the use of liquid electrolyte could be crucial, as the actual electrolyte used in real Li−oxygen batteries was found to be crucial for controlling battery performance and cyclability. Although there are in situ studies using AFM[17,18] and SPM[19] that captured successfully the lithium oxide film formation/decomposition in full LOB cycles, these surface probe techniques cannot detect the reaction at the interface between the reactant and the current collector. Also, although different types of volatile liquid-encapsulating cells have been used to investigate the electrochemical reaction at the electrolyte/electrode interface,[20−25] liquid-cell experiments has not been applied to LOB reactions. In this work, to confine the volatile liquid electrolyte and observe the LOB operations with TEM, we developed a liquid-confining cell (Figure 1a).

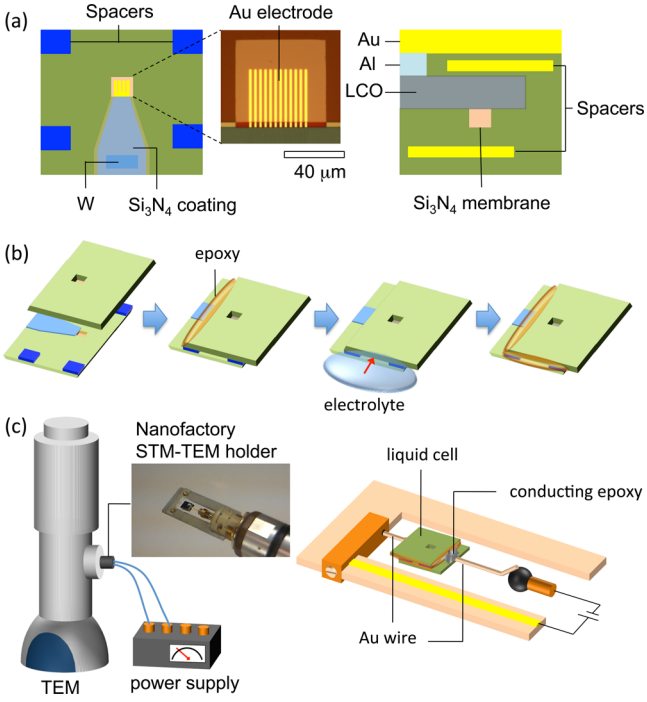

Figure 1. (a) Schematic illustration of the liquid confining cell. The optical micrograph image is the magnified view of the Au electrode patterned on the one side of the chip. $LiCoO_2$ (LCO) was sputtered on the Al film connected to the Au current collector as Li source. (b) Chip assembling procedure. (c) The chip is mounted on Nanofactory STM-TEM holder and inserted to TEM for the electrochemical test using external power supply.

The cell consists of two silicon chips with electron beam transparent Si_3N_4 membrane viewing windows. On one chip, gold electrodes were patterned at the window as a working electrode, and $LiCoO_2$ (LCO) thin film was sputtered on the Al current collector on the other chip. The details of the fabrication process and the chip configuration along with in situ experimental setup are explained in Supporting Information. The chips have spacers to secure space for electrolyte when the two chips are stacked in the assembling process described in Figure 1b. First, two of the four sides were sealed with epoxy glue leaving one side for electrolyte injection and the other for the air to escape. A solution of 1.0 M lithium bis-(trifluoromethane)sulfonimide salt (LiTFSI) dissolved in dimethyl sulfoxide (DMSO) was used as the electrolyte. After the electrolyte was bubbled with pure oxygen, the electrolyte was wicked into the cell through capillary action by contacting a droplet of the electrolyte to one of the openings. Finally, the two openings were sealed with epoxy glue. The electrolyte injection process including the oxygen bubbling was performed inside an argon-filled glovebox to avoid moisture. The assembled cell was mounted on a Nanofactory scanning tunneling microscopy (STM)−TEM holder for electrical biasing (Figure 1c).

Figure 2 shows sequential TEM images when (a) discharged at −2.0 V and (b) subsequently charged at 1.5 V with respect to

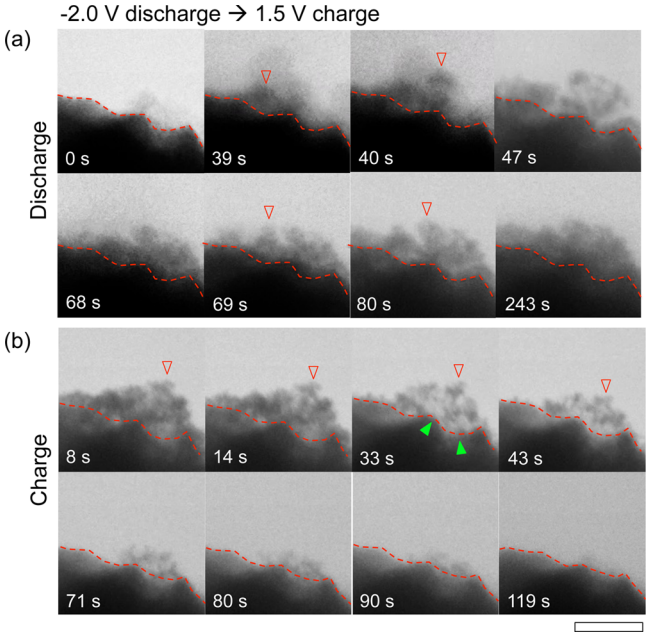

Figure 2. Sequential TEM images of the Li−O_2 battery reaction process under (a) discharge and (b) change process at −2.0 and 1.5 V vs LCO, respectively. The dashed line indicates the current collector surface. The scale bar is 100 nm. (See also Movies S1 and S2.)

the LCO counter electrode (see also Supporting Information Movies S1 and S2). As U^0(LCO) = 4.2 V vs Li/Li^+, this can be roughly assumed to be 2.2 and 5.7 V vs Li/Li^+, respectively, assuming low polarization at LCO and low long-range transport loss. Note that in our two electrode setup, it is difficult to determine if the LCO reached the stable reaction potential plateau although the amount of LCO loaded in the device was small with ∼0.98 μg at 0.098 mg/cm^2 (see Supporting Information for detail). Three-electrode setup with a stable reference electrode will be necessary to precisely measure the reaction potential, which we have not accomplished yet. At first, small particles formed on the gold current collector. As the reaction proceeded, particles accumulated on top of the previous reaction product as indicated by the open arrowheads in Figure 2a, indicating the reaction point was at the interface between the reaction product and the electrolyte. These particles kept accumulating, forming a film until it reached a thickness ∼100 nm at 80s. Here, the TEM video shows that the film was porous. After the film reached its maximum thickness, it ceased to grow further. However, the reaction product continued to fill the pores and a dense film was formed on the electrode eventually. This is because growth at the product/

DOI: 10.1021/acs.nanolett.5b03812
Nano Lett. 2015, 15, 8260−8265

electrolyte interface will not cease as long as a pore is open, and the growth is limited by lithium ion diffusivity.

Although the in situ observation allowed us to capture the reaction morphology evolution, it was difficult to identify the precise composition of the film in the presence of the electrolyte, as the electron diffraction and electron energy loss spectroscopy (EELS) qualities were poor. To determine the reaction product, we conducted ex situ analysis by selected-area electron diffraction using a vial cell and confirmed that Li_2O_2 was formed (see Supporting Information Figure S5) under identical conditions. The ex situ characterization also revealed that the film was the agglomerate of small particles like the in situ observations. It is known that Li_2O_2 is a bulk insulator and electron cannot tunnel into bulk Li_2O_2 deeper than ~5−10 nm.[26,27] However, the surface of Li_2O_2 is calculated to be electrically conductive.[28] Because the film consisted of Li_2O_2 nanoparticles touching each other, the percolating surfaces and the interfaces provided electron conduction paths from the current collector to the surface of the film and product−electrolyte interface, allowing the film to grow thicker than the ~10 nm limit.

Figure 2b shows the charging process during which Li_2O_2 decomposes. The film started to decompose from the Li_2O_2−current collector interface, and the decomposition created voids in the Li_2O_2 film near the current collector indicated by the green arrowheads in the figure. The film collapsed to fill the void, and the reaction continued to the full decomposition. Most of the time, the top-surface contour of Li_2O_2 (marked by open arrowheads in the figure) maintained but shifted down, like a sinking ship. This proves that the decomposition happens at the current collector/Li_2O_2 interface, and the decomposition is limited by electronic conduction.

Different behaviors were observed when discharge potential was varied. Figure 3 shows (a) the discharging and (b) the charging process at −2.5 and 1.5 V vs LCO (see also Supporting Information Movies S3 and S4), respectively. At the early stage of the discharge, small particles formed on the surface of the electrode as indicated by the arrowheads in the snapshots taken at 31s. Then the small particles started to deposit/accumulate on the electrode in a porous tree-like structure. And at the later stage of the reaction, the particles at the tip of the tree grew larger (arrows at 184 and 186 s in the figure) like blossoming flowers. Ex situ analysis revealed a formation of Li_2O particles at this discharge potential (see Supporting Information). Lower discharge potential or higher discharge rate creating lower oxygen content in the electrolyte leads to the increase of the Li_2O/Li_2O_2 ratio in the reaction product.[8,29] After the potential was switched to 1.5 V for charge, some particles were detached and swept away into the electrolyte. However, those remaining in contact with the current collector started to decompose at the current collector interface, similar to the −2.0 V ORR → 1.5 V OER reaction in Figure 2b. As a result, the porous tree structure collapsed at the root. Because the particles at the top part maintained their shape (filled arrowheads in the snapshots after 2 and 24 s in Figure 3b), decomposition near the current collector must be responsible for the collapse. The porous film continued to shrink and eventually completely disappeared. In the process, it became smaller fragments and rolled on the electrode (open arrowheads in 32−42 s snapshots), and they decomposed but only while they maintained contacts with the electrode.

The reaction was more violent at the lower discharge potential (larger overpotential). Figure 4 shows the nano-

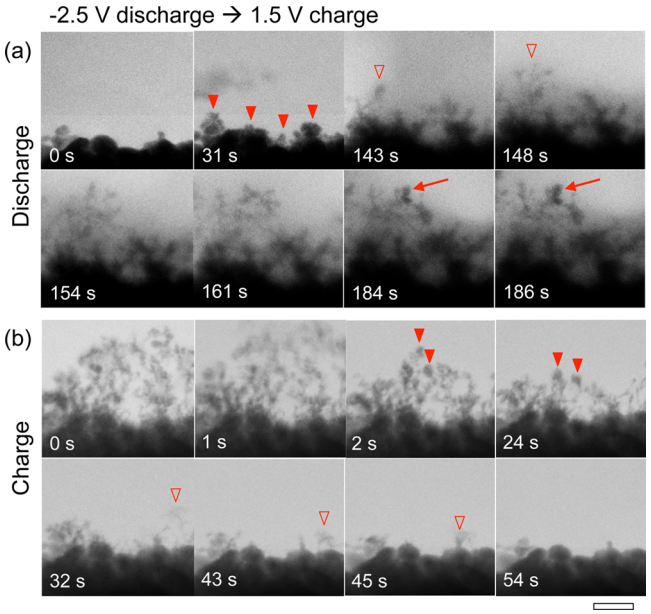

Figure 3. Sequential TEM images of the Li−O_2 battery reaction process under (a) discharge and (b) change process at −2.5 and 1.5 V vs LCO, respectively. The scale bar is 100 nm. (See also Movies S3 and S4.)

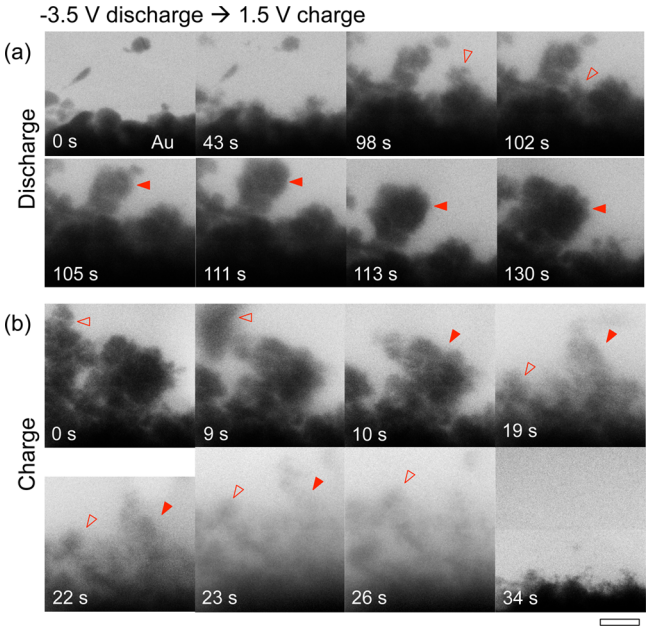

Figure 4. Sequential TEM images of the Li−O_2 battery reaction process under (a) discharge and (b) change process at −3.5 and 1.5 V vs LCO, respectively. The scale bar is 100 nm. (See also Movies S5 and S6.)

morphology evolution for (a) −3.5 V discharge and (b) 1.5 V charge (see also Supporting Information Movies S5 and S6). Similar to −2.0 V and −2.5 V discharge processes shown above, small particles were formed on the gold electrode at the beginning. These particles were not tightly adhered to the current collector, and changed their locations easily as indicated by open arrowhead in Figure 4a. Though some particles were

DOI: 10.1021/acs.nanolett.5b03812
Nano Lett. 2015, 15, 8260−8265

detached and swept away in the electrolyte, those that survived continued to grow larger (filled arrowheads in Figure 4a).

The particles formed during discharge started to decompose during charge (Figure 4b). However, similar to the discharge, most of the particles were detached from the electrode in the procedure and did not withstand the nanoscale flow agitations of the electrolyte. Such agitations are absent in the all-solid in situ TEM configuration.[16] There can be multiple reasons for the convective flow of the liquid, such as volume change of the solid parts, heat-induced convection, electroosmotic or electrocapillary forces, dielectrophoretic bending of the Si_3N_4 membrane induced by the electric field, and so forth. We believe such microscale flow agitations near the electrode surface are unavoidable in any actual battery and can indeed cause detachment of the electroactive particles, leading to the capacity loss. We call these detached particles in the liquid electrolyte that have lost electrical contact "flotsams", which is a cause of irreversibility, just like the solid−electrolyte interphase (SEI) debris that fall off high-capacity anode materials.[30] These completely insoluble Li_2O_2 "flotsams" in nonaqueous electrolyte[31] cannot be cycled and, therefore, would behave very much like SEI debris.

The above observation of the ORR and the OER processes at different potentials is summarized schematically in Figure 5. At low discharge potential (high ORR over potential), the reactant formed as nanoparticles at the initial stage. These particles were weakly bound to the electrode and other particles and easily swept away into the electrolyte. Only those maintaining the electric conduction path grew into the larger particles (selective growth). More rapid ORR reaction created lower O_2 concentration in the electrolyte near the reaction sites leading to the preferential formation of Li_2O. Increased discharge potential (smaller overpotential) seems to improve the adhesion between discharge product and Au and allowed most of the initially formed particles to remain in contact with the electrode. These small particles accumulated on the electrode, sometimes in a dendritic manner, forming a porous film. In charging, the OER process took place at the interface between the reactant and the current collector, causing the particles to detach and the film to collapse. When the discharge potential was further increased, a denser, less porous film was formed, although it consisted of nanoparticles of similar sizes as those observed at lower discharge potentials. Because the particles were closely packed in the film, they supported each other as the film decomposed at the interface with current collector, preventing them from floating away into the electrolyte. Note that the same bias potential was used for charging in the experiments. The results indicate that controlling the discharging process (despite the smaller overpotential and energy loss than in charging) to form densely packed (stable) film is critical for improving the cycling performance.

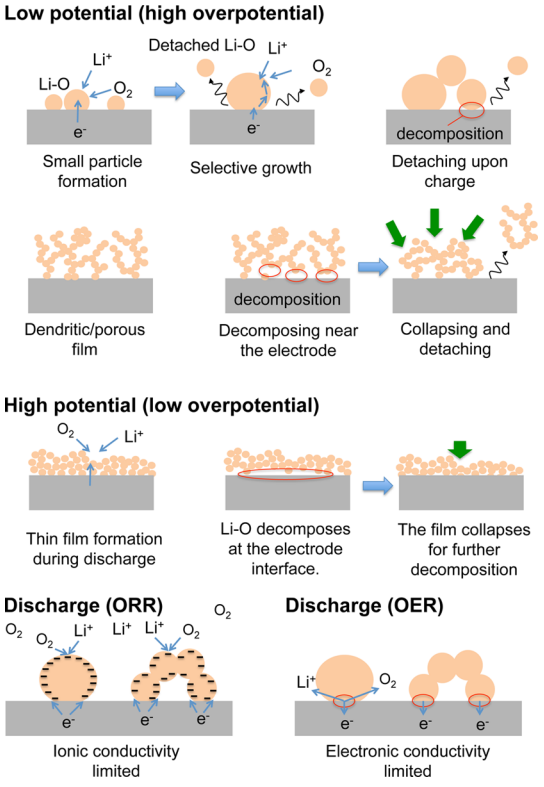

Figure 5. Schematic illustration explaining the discharge/charge mechanism in the Li−O_2 battery.

Our observations revealed an important spatial asymmetry (Figure 5 lower panel). The reaction locale of the discharge was at the reactant/electrolyte interface regardless of the applied potential, and the decomposition of the particles took place at the current collector/particle interface during charge. Although Li_2O_2 is a bulk insulator, the surface half-metallic states allow electrons to migrate on the surface.[28] These electrons combined with Li^+ and O_2 in the electrolyte to form Li_2O_2, and the film grew outward from the electrode, with the product/electrolyte interface being the primary reaction site, sometime forming dendritic trees. This is because surface electron conductivity is much faster than the Li^+ and O_2 diffusion in the electrolyte. Therefore, the ORR reaction was a Li^+/O_2 diffusion limited process. On the other hand, OER was observed to preferentially occur at the Li_2O_2/current collector interface, indicating that the kinetics were limited by the electron conductivity of the Li_2O_2 particles. This is consistent with in situ TEM observation of the Li_2O_2 oxidization under vacuum environment.[16] Such asymmetry in the reaction nanomorphologies (controlling electron transport length), as well as asymmetry in the chemical pathways,[12] contributes to the measured large asymmetry in the discharge/charge overpotential ΔU of LOB, with OER being the inherently more difficult process because the reaction has a tendency to cut itself off, by losing Li_2O_2/current collector true contact area[32] as the reaction progresses. For ORR, the more the reaction progresses and the larger the particles, the faster the total rate becomes due to larger reactant/electrolyte true contact area. We believe this contributes to the asymmetry in charging/discharging overpotential.

It is worth noting that the discharge (ORR) voltage used in this experiment was low (0.7−2.2 V vs Li/Li^+, assuming LCO potential as 4.2 V vs Li/Li^+). In this potential range, it is known that the Li_2O_2 particles do not grow into larger toroidal shape in DMSO solvent; instead, they form particulate film on the electrode.[33] This is consistent with our observation. The current density we detected during the constant voltage experiment was ~0.5 mA/cm^2 (see Supporting Information), which is well above the critical value for the Li_2O_2 morphological transition from the larger toroidal shape at low current density to the film at high current density discharge.[34] What we observed in our in situ TEM experiment agrees well with others' and our own ex situ observations. Note that the

DOI: 10.1021/acs.nanolett.5b03812
Nano Lett. 2015, 15, 8260−8265

discharge/charge rate used in our experiment is significantly faster than practical LOB. This may cause more porous oxide films and easier flotsam detachments observed in our in situ experiments, and the irreversible capacity loss by flotsam mechanism in the actual LOB should be smaller. Still, our observation suggests that the flotsam detachments of the oxide may affect the cyclability of LOB over tens and hundreds of cycles. Although liquid cell in situ TEM has its limitations that make it difficult to perform precise analysis of the samples immersed in the liquid, the material characterization can be complemented with ex situ analysis after removing the liquid from the cell. In other words, in situ analyses provide dynamic nanomorphology evolution of the reaction, and ex situ observation allows static and fine-scale identification of the products.

The present work may lead to improved LOB design. One of the important findings here is the detachment of the electroactive particles, forming "flotsams" during the reaction processes, which is difficult to capture with ex situ analysis. Because detached particles lead to irreversible capacity loss and cause poor cyclability of LOB, the electrode should be designed to prevent the detachment or to be able to recapture the floating Li_2O_2 particles. In this context, using mesoporous electrode is not only good for increasing reaction sites and reducing effective current density for higher capacity, it can also recapture the detached particles in the pores to improve the cycle life. To maximize the effect, one can design a structure with pores in different sizes distributed in a controlled manner. For example, larger pores (micron-sized) can be placed at the potential reaction sites near the O_2 path and the area can be surrounded with smaller pores (nanosized) to capture the detached reaction products during LOB operation.

In this work, we only present the data with DMSO solvent and low discharge potentials. However, observation of LOB reactions using various electrolyte and discharge/charge conditions is possible with the same technique. Also, we have demonstrated for the first time the in situ TEM observation of a three-phase-reaction involving gold electrode, lithium oxides, DMSO electrolyte and lithium salt, and O_2 gas using a liquid confining cell that we developed, which provided additional information regarding the asymmetric nanomorphology evolution (thus asymmetric charging/discharging overpotential) and battery degradation mechanisms. The technique described in this work is not limited to Li−oxygen battery, but it can also be potentially used in other applications where gas/liquid/solid electrochemical reactions are important.

■ ASSOCIATED CONTENT

Supporting Information

The Supporting Information is available free of charge on the ACS Publications website at DOI: 10.1021/acs.nanolett.5b03812.

Experimental procedures and additional data, figures, and tables. (PDF)

All movies recorded at 2 frames/s and played at 10× original speed.

Movie S1: Discharged at −2.0 V vs LCO. (MOV)
Movie S2: Charged at 1.5 V vs LCO after −2.0 V discharge. (MOV)
Movie S3: Discharged at −2.5 V vs LCO. (MOV)
Movie S4: Charged at 1.5 V vs LCO after −2.5 V discharge. (MOV)
Movie S5: Discharged at −3.5 V vs LCO. (MOV)
Movie S6: Charged at 1.5 V vs LCO after −3.5 V discharge. (MOV)

■ AUTHOR INFORMATION

Corresponding Author

*E-mail: liju@mit.edu.

Notes

The authors declare no competing financial interest.

■ ACKNOWLEDGMENTS

We acknowledge financial support from Honda R&D Co. Ltd. We are also grateful for discussions with Prof. Sanjeev Mukerjee.

■ REFERENCES

(1) Scrosati, B.; Garche, J. Lithium Batteries: Status, Prospects and Future. *J. Power Sources* **2010**, *195*, 2419−2430.

(2) Girishkumar, G.; McCloskey, B.; Luntz, A. C.; Swanson, S.; Wilcke, W. Lithium−Air Battery: Promise and Challenges. *J. Phys. Chem. Lett.* **2010**, *1*, 2193−2203.

(3) Zheng, J. P.; Liang, R. Y.; Hendrickson, M.; Plichta, E. J. Theoretical Energy Density of Li−Air Batteries. *J. Electrochem. Soc.* **2008**, *155*, A432−A437.

(4) Débart, A.; Bao, J.; Armstrong, G.; Bruce, P. G. An O2 Cathode for Rechargeable Lithium Batteries: The Effect of a Catalyst. *J. Power Sources* **2007**, *174*, 1177−1182.

(5) Débart, A.; Paterson, A. J.; Bao, J.; Bruce, P. G. α-MnO2 Nanowires: A Catalyst for the O2 Electrode in Rechargeable Lithium Batteries. *Angew. Chem., Int. Ed.* **2008**, *47*, 4521−4524.

(6) Lu, Y.-C.; Xu, Z.; Gasteiger, H. A.; Chen, S.; Hamad-Schifferli, K.; Shao-Horn, Y. Platinum−Gold Nanoparticles: A Highly Active Bifunctional Electrocatalyst for Rechargeable Lithium−Air Batteries. *J. Am. Chem. Soc.* **2010**, *132*, 12170−12171.

(7) Read, J. Characterization of the Lithium/Oxygen Organic Electrolyte Battery. *J. Electrochem. Soc.* **2002**, *149*, A1190.

(8) Zhang, S. S.; Foster, D.; Read, J. Discharge Characteristic of a Non-Aqueous Electrolyte Li/O2 Battery. *J. Power Sources* **2010**, *195*, 1235−1240.

(9) Zhang, G. Q.; Zheng, J. P.; Liang, R.; Zhang, C.; Wang, B.; Hendrickson, M.; Plichta, E. J. Lithium−Air Batteries Using SWNT/CNF Buckypapers as Air Electrodes. *J. Electrochem. Soc.* **2010**, *157*, A953.

(10) Cheng, H.; Scott, K. Carbon-Supported Manganese Oxide Nanocatalysts for Rechargeable Lithium−air Batteries. *J. Power Sources* **2010**, *195*, 1370−1374.

(11) Bruce, P. G.; Freunberger, S. A.; Hardwick, L. J.; Tarascon, J.-M. Li-O2 and Li-S Batteries with High Energy Storage. *Nat. Mater.* **2011**, *11*, 19−29.

(12) Peng, Z.; Freunberger, S. A.; Hardwick, L. J.; Chen, Y.; Giordani, V.; Bardé, F.; Novák, P.; Graham, D.; Tarascon, J.-M.; Bruce, P. G. Oxygen Reactions in a Non-Aqueous Li+ Electrolyte. *Angew. Chem., Int. Ed.* **2011**, *50*, 6351−6355.

(13) Abraham, K. M. A Polymer Electrolyte-Based Rechargeable Lithium/Oxygen Battery. *J. Electrochem. Soc.* **1996**, *143*, 1.

(14) Huang, J. Y.; Zhong, L.; Wang, C. M.; Sullivan, J. P.; Xu, W.; Zhang, L. Q.; Mao, S. X.; Hudak, N. S.; Liu, X. H.; Subramanian, A.; et al. In Situ Observation of the Electrochemical Lithiation of a Single SnO2 Nanowire Electrode. *Science* **2010**, *330*, 1515−1520.

(15) Liu, X. H.; Liu, Y.; Kushima, A.; Zhang, S.; Zhu, T.; Li, J.; Huang, J. Y. In Situ TEM Experiments of Electrochemical Lithiation and Delithiation of Individual Nanostructures. *Adv. Energy Mater.* **2012**, *2*, 722−741.

(16) Zhong, L.; Mitchell, R. R.; Liu, Y.; Gallant, B. M.; Thompson, C. V.; Huang, J. Y.; Mao, S. X.; Shao-Horn, Y. In Situ Transmission Electron Microscopy Observations of Electrochemical Oxidation of Li2O2. *Nano Lett.* **2013**, *13*, 2209−2214.

DOI: 10.1021/acs.nanolett.5b03812
Nano Lett. 2015, 15, 8260−8265

(17) Wen, R.; Hong, M.; Byon, H. R. In Situ AFM Imaging of Li−O2 Electrochemical Reaction on Highly Oriented Pyrolytic Graphite with Ether-Based Electrolyte. *J. Am. Chem. Soc.* **2013**, *135*, 10870−10876.
(18) Wen, R.; Byon, H. R. In Situ Monitoring of the Li−O2 Electrochemical Reaction on Nanoporous Gold Using Electrochemical AFM. *Chem. Commun.* **2014**, *50*, 2628−2631.
(19) Kreidler, E.; Xu, Q.; Omichi, K.; Brooks, C. In-Situ Scanning Probe Microscopy for Observing Electrode Surfaces Under Operating Conditions. *ECS Meet. Abstr.* **2013**, *MA2013-02*, 456−456.
(20) de Jonge, N.; Ross, F. M. Electron Microscopy of Specimens in Liquid. *Nat. Nanotechnol.* **2011**, *6*, 695−704.
(21) Liao, H.-G.; Cui, L.; Whitelam, S.; Zheng, H. Real-Time Imaging of Pt3Fe Nanorod Growth in Solution. *Science* **2012**, *336*, 1011−1014.
(22) Radisic, A.; Ross, F. M.; Searson, P. C. In Situ Study of the Growth Kinetics of Individual Island Electrodeposition of Copper. *J. Phys. Chem. B* **2006**, *110*, 7862−7868.
(23) Sacci, R. L.; Black, J. M.; Balke, N.; Dudney, N. J.; More, K. L.; Unocic, R. R. Nanoscale Imaging of Fundamental Li Battery Chemistry: Solid-Electrolyte Interphase Formation and Preferential Growth of Lithium Metal Nanoclusters. *Nano Lett.* **2015**, *15*, 2011−2018.
(24) Sun, M.; Liao, H.-G.; Niu, K.; Zheng, H. Structural and Morphological Evolution of Lead Dendrites during Electrochemical Migration. *Sci. Rep.* **2013**, *3*, 3227.
(25) Zeng, Z.; Liang, W.-I.; Liao, H.-G.; Xin, H. L.; Chu, Y.-H.; Zheng, H. Visualization of Electrode−Electrolyte Interfaces in LiPF6/EC/DEC Electrolyte for Lithium Ion Batteries via in Situ TEM. *Nano Lett.* **2014**, *14*, 1745−1750.
(26) Viswanathan, V.; Thygesen, K. S.; Hummelshøj, J. S.; Nørskov, J. K.; Girishkumar, G.; McCloskey, B. D.; Luntz, A. C. Electrical Conductivity in Li2O2 and Its Role in Determining Capacity Limitations in Non-Aqueous Li-O2 Batteries. *J. Chem. Phys.* **2011**, *135*, 214704.
(27) Radin, M. D.; Siegel, D. J. Charge Transport in Lithium Peroxide: Relevance for Rechargeable Metal−air Batteries. *Energy Environ. Sci.* **2013**, *6*, 2370−2379.
(28) Radin, M. D.; Tian, F.; Siegel, D. J. Electronic Structure of Li2O2 {0001} Surfaces. *J. Mater. Sci.* **2012**, *47*, 7564−7570.
(29) Read, J. Characterization of the Lithium/Oxygen Organic Electrolyte Battery. *J. Electrochem. Soc.* **2002**, *149*, A1190−A1195.
(30) Li, S.; Niu, J.; Zhao, C.; So, K.; Wang, C.; Wang, C. A.; Li, J. High-Rate Aluminium Yolk-Shell Nanoparticle Anode for Li-Ion Battery with Long Cycle Life and Ultrahigh Capacity. *Nat. Commun.* **2015**, *6*, 7872.
(31) McCloskey, B. D.; Scheffler, R.; Speidel, A.; Bethune, D. S.; Shelby, R. M.; Luntz, A. C. On the Efficacy of Electrocatalysis in Nonaqueous Li−O2 Batteries. *J. Am. Chem. Soc.* **2011**, *133*, 18038−18041.
(32) Guo, W.; Wang, Z.; Li, J. Diffusive versus Displacive Contact Plasticity of Nanoscale Asperities: Temperature- and Velocity-Dependent Strongest Size. *Nano Lett.* **2015**, *15*, 6582−6585.
(33) Johnson, L.; Li, C.; Liu, Z.; Chen, Y.; Freunberger, S. A.; Ashok, P. C.; Praveen, B. B.; Dholakia, K.; Tarascon, J.-M.; Bruce, P. G. The Role of LiO2 Solubility in O2 Reduction in Aprotic Solvents and Its Consequences for Li−O2 Batteries. *Nat. Chem.* **2014**, *6*, 1091−1099.
(34) Adams, B. D.; Radtke, C.; Black, R.; Trudeau, M. L.; Zaghib, K.; Nazar, L. F. Current Density Dependence of Peroxide Formation in the Li−O2 Battery and Its Effect on Charge. *Energy Environ. Sci.* **2013**, *6*, 1772−1778.

DOI: 10.1021/acs.nanolett.5b03812
Nano Lett. 2015, 15, 8260−8265

Supporting Information for

"Charging/Discharging Nanomorphology Asymmetry and Rate-Dependent Capacity Degradation in Li-Oxygen Battery"

Akihiro Kushima[1], Tetsuya Koido[2], Yoshiya Fujiwara[2], Nariaki Kuriyama[3], Nobuhiro Kusumi[2], and Ju Li[1,4*]

[1] Department of Nuclear Science and Engineering, Massachusetts Institute of Technology, Cambridge, MA 02139
[2] Honda R&D Co. Ltd., Automobile R&D Center, Wako-shi, Saitama 351-0193, Japan
[3] Honda R&D Co. Ltd., Fundamental Technology Research Center, Wako-shi, Saitama 351-0188, Japan,
[4] Department of Materials Science and Engineering, Massachusetts Institute of Technology, Cambridge, MA 02139

In-situ liquid cell experiment

We designed a liquid confining cell for in-situ transmission electron microscopy (TEM) observation of the electrochemical reactions. The cell consists of two chips (one with Au electrode and the other with $LiCoO_2$ film). These chips were fabricated on four-inch Si wafer. The procedure is schematically shown in Fig. S1. First, 70 nm Si_3N_4 membrane was deposited on a wafer by low-pressure chemical vapor deposition (LP-CVD). Then a current collector was deposited. Ti/Au/Cr was used for the one with Au electrode (Cr was later removed) and Al was selected as the current collector for the chip with LCO film. After the Au was deposited as the working electrode, Si_3N_4 was deposited on the Au electrode outside the membrane window area as a passivation layer by plasma-enhanced (PE) CVD to prevent undesired side reactions and current consumptions during the discharge process. For the LCO chip, LCO film was deposited on the Al current collector followed by 500 °C annealing. The membrane window was created by Si backside etching → front side surface protection → silicon etching → removing protection layer. Finally, the wafer was diced to individual chips. Optical microscopy images of the chips are shown in Fig. S2. The material selection and the thickness for the chip fabrication are summarized in Table S1, and the geometry of the gold electrode on the liquid confining cell is shown in Fig. S3.

After the cell was assembled and the O_2 bubbled electrolyte was injected, we mounted the cell on Nanofactory scanning tunneling microscopy (STM) - TEM holder for the observation as schematically illustrated in Fig. S4. Here, gold rods were glued on the electrode pads of the cell using conducting epoxy (Circuitworks, CW2400) for mounting the cell on the holder. JEOL 2010F with 200 kV acceleration voltage was used for the in-situ TEM experiment.

We used dimethyl sulfoxide (DMSO) as the electrolyte solvent. The O_2 solubility of the DMSO is 6.44×10^{-3} g/100g, and the amount of electrolyte stored in the device can be roughly estimated to be ~0.4×10^{-6} cm^3 (0.44×10^{-6} g). Therefore, amount of O_2 in the

DMSO electrolyte can be calculated to be, 2.83 x 10^{-9} g (8.8 x 10^{-11} mol), which can produce 4.04 x 10^{-9} g or 1.74 x 10^{3} μm^3 of Li_2O_2. Since the surface area of the gold electrode in the chip is 1.16 x10^{3} μm^2, this can produce ~1.5 μm thick Li_2O_2 substrate on the electrode surface if uniformly deposited, which is enough to be observed by the in-situ liquid cell TEM. In reality, the deposition took place at the certain sites on the electrode where Li_2O_2 can preferentially deposit, and the particles were easily located in our experiments.

Ex-situ analysis

We conducted ex-situ characterization of the reaction products using a vial cell as shown in Fig. S5a. Here, we used the liquid confining cell with a gold electrode as the working electrode, $LiCoO_2$ (LCO) slurry pasted on Al foil as the counter electrode, and 1M LiTFSI in DMSO as the electrolyte. We performed O_2 gas bubbling in the electrolyte for five minutes before immersing the electrodes in the electrolyte and applying a bias voltage on the chip electrode with respect to the LCO counter electrode for 10 minutes. Then, the chip was extracted from the electrolyte and rinsed with DME to remove residual electrolyte from the chip for the TEM characterization of the reactant.

Figure S5b shows the TEM image of the reaction product after discharge at -2.0 V vs. LCO. These particles had a fine nano-crystalline or granular structure. The electron diffraction pattern (EDP) of the particles indicates they are Li_2O_2. Figure S5c depicts the reaction product at -2.5 V vs. LCO discharge. The appearance of the reactant is similar to that of the -2.0 V discharge products. However, the EDP reveals they are Li_2O. Combining these ex-situ characterizations, we conclude the stable film formed at -2.0 V vs. LCO discharge was Li_2O_2, and rapidly grown particles at -2.5 V and -3.5V vs. LCO were Li_2O. In the TEM analysis we used the largest spot size and spread the beam to reduce the beam current as much as possible and took the electron diffraction patterns to avoid electron beam damage to the Li_2O_2, and the TEM images were taken at low magnification to avoid strong beam exposed on to the sample.

Current density

Figure S6 shows current profiles during discharge and charge at different voltages. For all voltages used in this work, the current decayed rapidly to a constant value (~5 nA) although the initial current are higher for the lower discharge potentials. As shown in Fig. S3, there are 12 Au electrodes with width W = 2.0 μm and length L = 40 μm on the chip. Therefore, the total electrode area can be estimated as 960 μm^2. This gives a current density of ~0.5 mA/cm^2 during the discharge. Similarly, the current decays during charge. This is most significant when charged after discharged at -3.5 V vs. LCO although the same charge potential of 1.5 V vs. LCO was used in all three cases. The coulombic efficiency are ~16%, 40%, and 44%, for charging after -3.5 V, -2.5 V, -2.0 V discharge, respectively. The low efficiency at lower discharge potential agrees with the observation of detaching particles. It is worth noting that our experiment was conducted at constant voltage and the duration of discharge/charge affects the total electric current as DMSO may decompose with electrolyte side reactions. Constant current experiment with a cut-off potential is necessary to precisely analyze the efficiency.

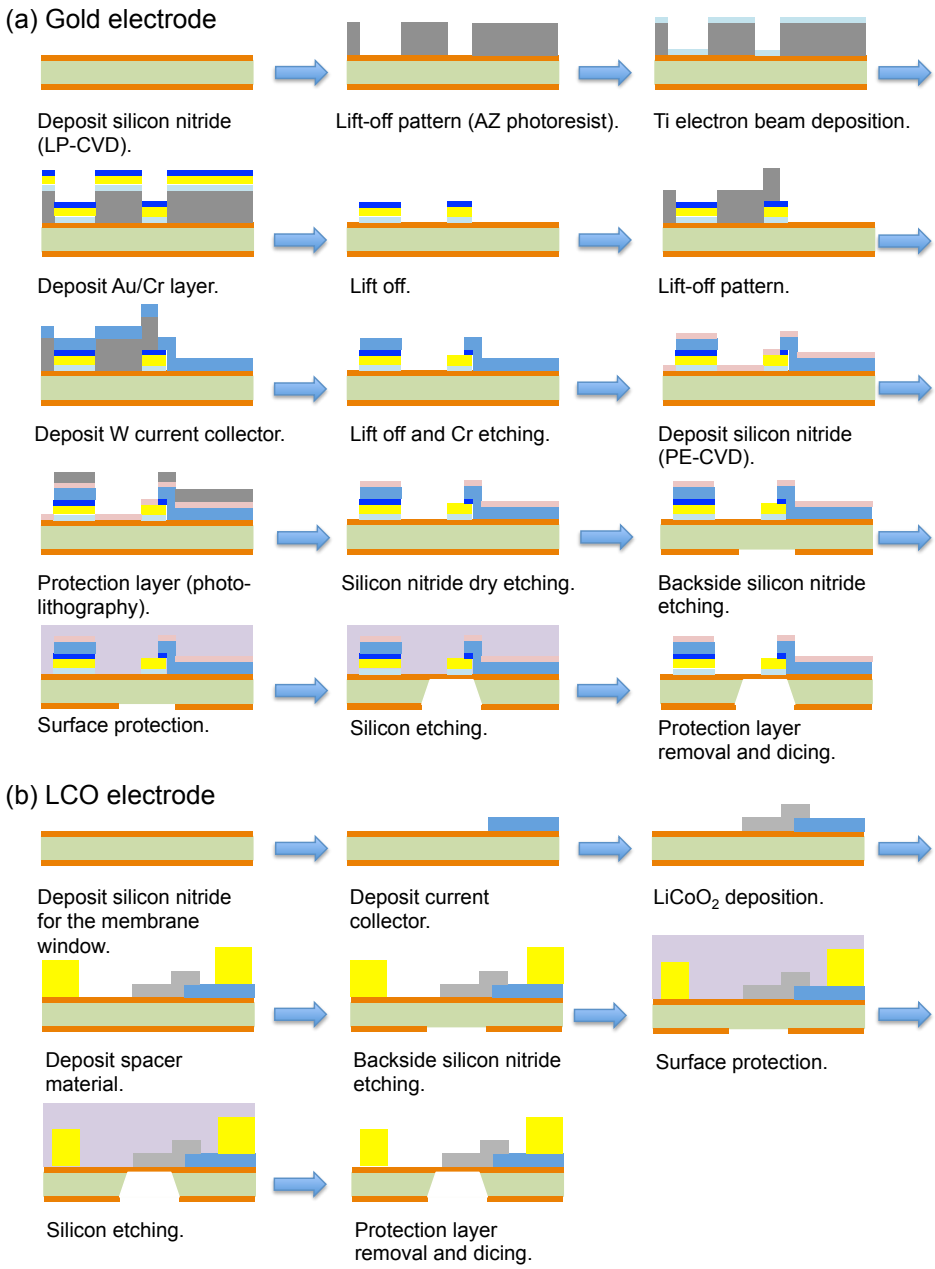

Figure S1. Schematic illustration explaining fabrication process of the liquid cell chip for (a) gold and (b) LCO electrode.

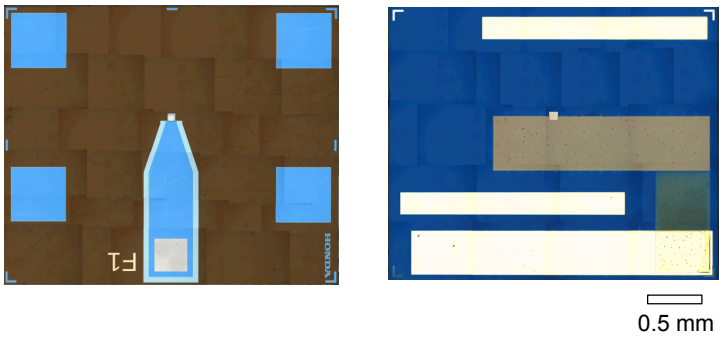

Figure S2. Optical micrographs of the liquid cell with gold electrode (left) and LCO film (right).

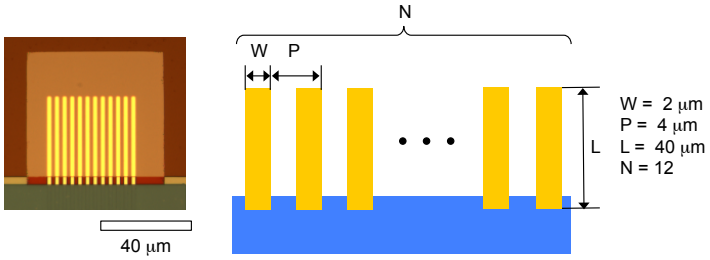

Figure S3. Optical micrograph of the gold electrode on the liquid confining cell (left) and the geometry (right).

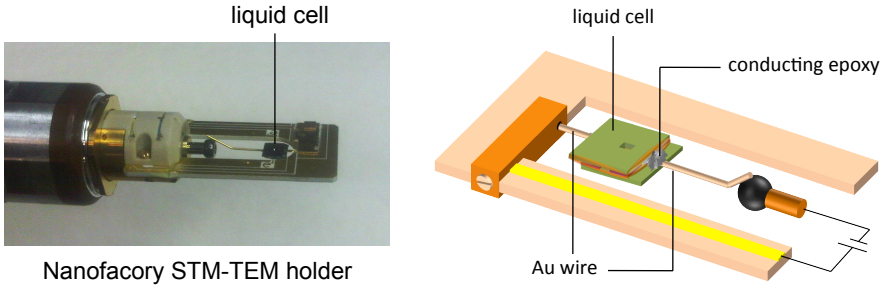

Figure S4. Liquid cell mounted on Nanofactory STM-TEM holder. Optical micrograph image (left) and schematics (right).

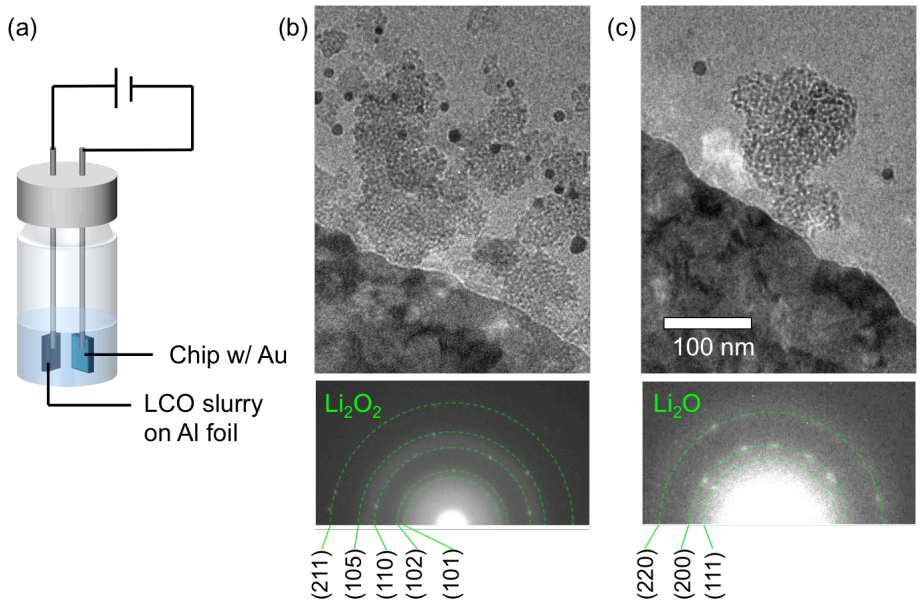

Figure S5. (a) Ex-situ vial experiment setup. (b) Discharge product at -2.0 V vs. LCO. (c) Discharge product at -2.5 V vs. LCO.

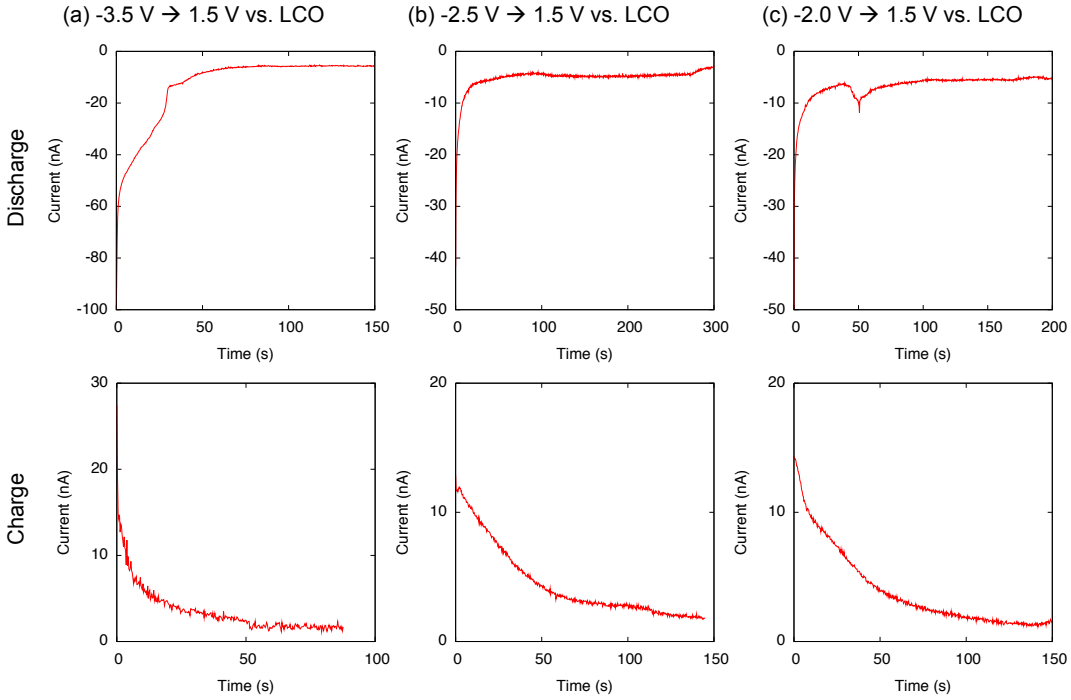

Figure S6. Change in the electric current during discharge (upper panels) and charge (lower panels) using (a) -3.5 V, (b) -2.5 V, and (c) -2.0 V discharge and 1.5 V charge voltage with respect to LCO.

Table S1. Design parameters of the liquid cell.

	Au electrode	LCO film
Active material	Ti/Au : 15/40 nm	$LiCoO_2$: 200 nm
Current collector	Cr/Au/Cr : 15/20/15 nm	Al : 100 nm
Spacer	Ti/Au/Cr/W/Si_3N_4 : 15/40/15/70/70 nm (210 nm)	Au/Cr : 200/50 nm
Passivation layer	Si_3N_4 : 70 nm	N/A